ACS Catalysis

Research Article

pubs.acs.org/acscatalysis

Trends in Formic Acid Decomposition on Model Transition Metal Surfaces: A Density Functional Theory study

Jeffrey A. Herron, Jessica Scaranto, Peter Ferrin, Sha Li, and Manos Mavrikakis*

Department of Chemical and Biological Engineering, University of Wisconsin − Madison, 1415 Engineering Drive, Madison, Wisconsin 53706, United States

Supporting Information

ABSTRACT: We present a first-principles, self-consistent periodic density functional theory (PW91-GGA) study of formic acid (HCOOH) decomposition on model (111) and (100) facets of eight fcc metals (Au, Ag, Cu, Pt, Pd, Ni, Ir, and Rh) and (0001) facets of four hcp (Co, Os, Ru, and Re) metals. The calculated binding energies of key formic acid decomposition intermediates including formate (HCOO), carboxyl (COOH), carbon monoxide (CO), water (H_2O), carbon dioxide (CO_2), hydroxyl (OH), carbon (C), oxygen (O), and hydrogen (H; H_2) are presented. Using these energetics, we develop thermochemical potential energy diagrams for both the carboxyl-mediated and the formate-mediated dehydrogenation mechanisms on each surface. We evaluate the relative stability of COOH, HCOO, and other isomeric intermediates (i.e., CO + OH, CO_2 + H, CO + O + H) on these surfaces. These results provide insights into formic acid decomposition selectivity (dehydrogenation versus dehydration), and in conjunction with calculated vibrational frequency modes, the results can assist with the experimental search for the elusive carboxyl (COOH) surface intermediate. Results are compared against experimental reports in the literature.

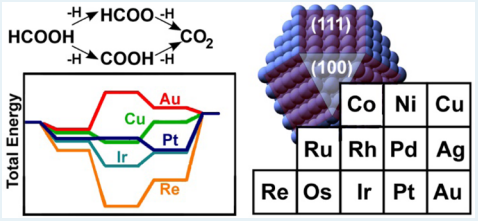

KEYWORDS: *formic acid, density functional theory, structure sensitivity, dehydrogenation, thermochemistry, selectivity*

1. INTRODUCTION

Formic acid is a byproduct of the catalytic conversion of lignocellusoic biomass to levulinic acid, an important platform molecule.[1,2] Decomposition of this HCOOH over a heterogeneous catalyst to produce hydrogen (and carbon dioxide) is an attractive method of utilizing HCOOH to hydrogenate levulinic acid to gamma-valerolactone (GVL), without the use of an external hydrogen source. Though formic acid decomposition has been studied extensively,[3−10] the reaction mechanism remains poorly understood.

Formic acid can decompose via two principal routes: dehydrogenation (HCOOH → CO_2 + H_2) or dehydration (HCOOH → CO + H_2O). These reactions are coupled by the water gas shift reaction (WGSR) (CO + H_2O → CO_2 + H_2). In order to produce pure hydrogen, the selectivity toward the dehydrogenation reaction is important, partly because most Pt-group metals would be, to a large extent, poisoned by CO if the dehydration path was to dominate. The dehydrogenation mechanism has been the subject of a wide scientific debate. Sachtler et al. proposed a formate mechanism, where formic acid dissociatively adsorbs to give formate (HCOO), which is then dehydrogenated to carbon dioxide.[4] The same authors plotted the catalytic activity of metals versus heat of formation of bulk metal-formates, arriving at a volcano curve with Pt and Ir near the peak (i.e., most active). Furthermore, spectroscopic evidence has shown the existence of formate on a number of supported metal catalysts including Re,[11] Ir,[12] Rh,[12] Co,[13] Au,[14] and Cu,[15] as well as on single crystals: Ru(0001),[16] Rh(111),[17] Co(10$\bar{1}$0),[18] Pt(111),[19,20] Pd(111),[21] Ni(110),[22,23] Ag(110),[24] Cu(110),[25] and Cu(100).[26] Additionally, Silbaugh and co-workers studied formic acid decomposition to formate on clean and O-covered Pt(111) using single-crystal adsorption calorimetry.[27] However, studies by Mavrikakis and co-workers have shown, via a combination of experimental reaction kinetics studies, density functional theory (DFT) calculations, and microkinetic modeling, that, while formate is present on the surface of Cu[28] and Pt[29] catalysts during the WGSR, formate in those cases is only a spectator species. Instead, the WGSR proceeds via a carboxyl (COOH)-mediated mechanism. Lin et al.[30] studied WGSR on (111) surfaces of Co, Ni, Cu, Rh, Pd, Ag, Ir, Pt, and Au using DFT calculations and found that COOH formation from HCOOH is more difficult than HCOO formation, and that COOH decomposition into CO_2 and H is easier than HCOO decomposition. They suggested that this is the reason why HCOO is the experimentally most observed intermediate.

A number of theoretical studies[31−33] have investigated a carboxyl-mediated formic acid decomposition. In this mechanism, the C−H bond in formic acid is activated first (instead of the O−H bond) forming carboxyl, which is then dehydrogenated to CO_2. A comparison between these two mechanisms is shown in Scheme 1.

Several theoretical studies of formic acid decomposition (and oxidation) on specific surfaces exist in the literature,[31−35] but

Received: May 19, 2014
Revised: September 15, 2014
Published: October 21, 2014

 © 2014 American Chemical Society dx.doi.org/10.1021/cs500737p | ACS Catal. 2014, 4, 4434−4445

Scheme 1. Pathways for Formic Acid Dehydrogenation

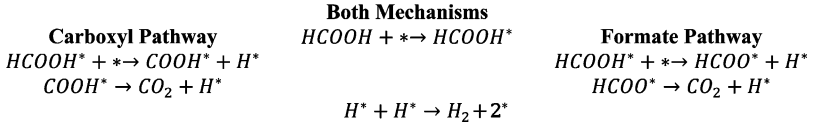

Table 1. Binding Energies of HCOOH, HCOO, COOH, CO, OH, O, C, and H on Model Transition Metal Surfaces[a]

	binding energy (eV)															
metal	HCOOH		HCOO		COOH		CO		OH		O		C		H	
	(111)[b]	(100)	(111)[b]	(100)	(111)[b]	(100)	(111)[b]	(100)	(111)[b]	(100)	(111)[b]	(100)	(111)[b]	(100)	(111)[b]	(100)
Au	−0.16	**−0.22**	−1.78	**−2.12**	−1.35	**−1.56**	−0.26	**−0.61**	−1.56	**−2.16**	−2.47	**−2.73**	−3.68	**−4.44**	−2.04	−2.22
Ag	−0.18	**−0.23**	−2.31	**−2.69**	−1.19	**−1.45**	−0.10	**−0.32**	−2.28	**−2.73**	−3.16	**−3.75**	−3.15	**−4.16**	**−2.07**	−2.01
Cu	−0.23	**−0.36**	−2.76	**−3.06**	−1.52	**−1.89**	−0.72	**−0.83**	−2.69	**−3.10**	−4.14	**−4.71**	−4.30	**−5.79**	**−2.38**	−2.37
Pt	−0.37	**−0.52**	−2.35	**−2.58**	−2.40	**−2.73**	−1.74	**−2.11**	−2.11	**−2.71**	−3.73	**−3.89**	−6.57	**−7.40**	−2.70	**−2.91**
Pd	−0.39	**−0.50**	−2.34	**−2.54**	−2.19	**−2.50**	−1.95	**−1.96**	−2.22	**−2.57**	−3.73	**−3.87**	−6.46	**−7.58**	**−2.83**	−2.78
Ni	−0.32	**−0.58**	−2.80	**−3.27**	−2.25	**−2.62**	−1.90	**−2.04**	−2.98	**−3.31**	−4.94	**−5.38**	−6.38	**−7.95**	**−2.81**	−2.78
Ir	−0.43	**−0.72**	−2.94	**−3.33**	−2.63	**−3.22**	−1.83	**−2.38**	−2.60	**−3.34**	−4.69	**−5.07**	−6.88	**−8.04**	−2.73	**−3.01**
Rh	−0.49	**−0.67**	−2.94	**−3.24**	−2.58	**−3.09**	−1.92	**−2.23**	−2.72	**−3.25**	−4.74	**−5.07**	−7.05	**−8.26**	−2.82	**−2.88**
Co	−0.33	--	−2.95	--	−2.25	--	−1.83	--	−3.13	--	−5.23	--	−6.59	--	−2.98	--
Os	−0.69	--	−3.62	--	−3.05	--	−2.10	--	−3.05	--	−5.47	--	−7.37	--	−2.81	--
Ru	−0.81	--	−3.50	--	−3.00	--	−1.98	--	−3.22	--	−5.29	--	−6.99	--	−2.90	--
Re	−0.64	--	−3.55	--	−2.83	--	−1.92	--	−3.72	--	−6.69	--	−7.47	--	−3.04	--

[a]For each adsorbate, the surface with the stronger binding energy is indicated in bold font. Metals are arranged according to periodic table group in descending order and, within each group, by decreasing atomic number. The respective binding energies calculated non self-consistently in RPBE are provided in Table S2. [b]These are (0001) facets for Co, Ru, Re, and Os.

not over a range of surfaces (elemental composition and facet), except for recent work by Yoo and co-workers.[36] Here, we present a first-principles, periodic, self-consistent density functional theory study of formic acid decomposition on model transition metal surfaces via the formate and carboxyl mechanisms. In this study, we limit our analysis to the dehydrogenation reaction, rather than the dehydration reaction, though we comment briefly on the selectivity between these two paths in section 3.6. Experiments have demonstrated that the activity of a formic acid decomposition catalyst is not merely a function of the metal. Rather, depending on the metal, there may be additional factors including particle size[37,38] and thereby structure sensitivity and support effects.[11,39,40] In the present study, we offer some initial insights on the effect of metal and the structure sensitivity of this reaction based on a simple thermochemical analysis (excluding entropic contributions) of the reaction pathways. These insights can provide guidance for the design of improved formic acid dehydrogenation catalysts.[36,41]

2. METHODS

Periodic, self-consistent density functional theory calculations (DFT) were performed with the PW91-GGA[42] exchange correlation functional using DACAPO.[43,44] The catalysts were modeled with the (111) and (100) facets of face-centered cubic metals (Au, Ag, Cu, Pt, Pd, Ni, Ir, Rh) and the (0001) facets of hexagonal-close-packed metals (Co, Os, Ru, Re). The optimized bulk lattice constants (experimental value[45] in parentheses) are Ag 4.14 Å (4.09 Å), Au 4.18 Å (4.08 Å), Co 2.50 Å (2.51 Å), Cu 3.67 Å (3.62 Å), Ir 3.86 Å (3.83 Å), Ni 3.52 Å (3.52 Å), Os 2.74 Å (2.73 Å), Pd 3.99 Å (3.89 Å), Pt 4.00 Å (3.92 Å), Re 2.76 Å (2.76 Å), Rh 3.83 Å (3.80 Å), Ru 2.74 Å (2.71 Å). For hcp metals, we used an idealized c/a ratio of 1.63—the experimental values are Co (1.623), Os (1.606), Ru (1.582), and Re (1.614).[45] The binding energies of HCOOH, HCOO, COOH, CO, OH, O, C, and H were calculated on 3 × 3 surface unit cells, corresponding to 1/9 ML coverage. For the close-packed (111) and (0001) facets, the metal slabs consist of three layers with all slab atoms fixed at their bulk truncated positions, as our tests indicated that surface relaxation in close packed surfaces has a negligible effect on the resulting energetics. For the more open (100) facet, the metal slabs consist of four layers with the top two layers of atoms fully relaxed. Five equivalent layers of vacuum are inserted between successive slabs. Convergence tests suggested that the surface Brillouin zone of the (111) and (0001) facets should be sampled at 18 special Chadi-Cohen k-points for Au, Ag, and Cu, and at 6 special k-points for Pt, Pd, Ni, Rh, Ir, Co, Os, Ru, and Re.[46] The (100) facets were sampled using a 4 × 4 × 1 Monkhorst−Pack *k*-point mesh.[47] All calculation parameters have been verified to ensure convergence of calculated binding energies. The ionic cores are described by ultrasoft Vanderbilt pseudopotentials.[48] Adsorption is permitted on only one of the two exposed surfaces, and the dipole moment[49,50] is adjusted accordingly. The Kohn−Sham one-electron states are expanded in a series of plane waves with an energy cutoff of 25 Ry. Calculations on Ni and Co surfaces included spin polarization.

The binding energies (*BE*) of adsorbates are calculated with the formula:

$$BE = E_{\text{total}} - E_{\text{substrate}} - E_{\text{gas-phase absorbate}}$$

where E_{total} is the total energy of the adsorbate/slab system, $E_{\text{substrate}}$ is the total energy of the clean slab, and $E_{\text{gas-phase adsorbate}}$ is the total energy of the adsorbate in the gas phase. We note that we do not account for van der Waals interactions in our calculations, but we expect that these effects would be relatively uniform across all metal surfaces studied. A negative binding energy indicates exothermic adsorption. The harmonic vibrational frequencies of an adsorbate are determined from the diagonalization of mass-weighted Hessian matrix. The second

dx.doi.org/10.1021/cs500737p | ACS Catal. 2014, 4, 4434−4445

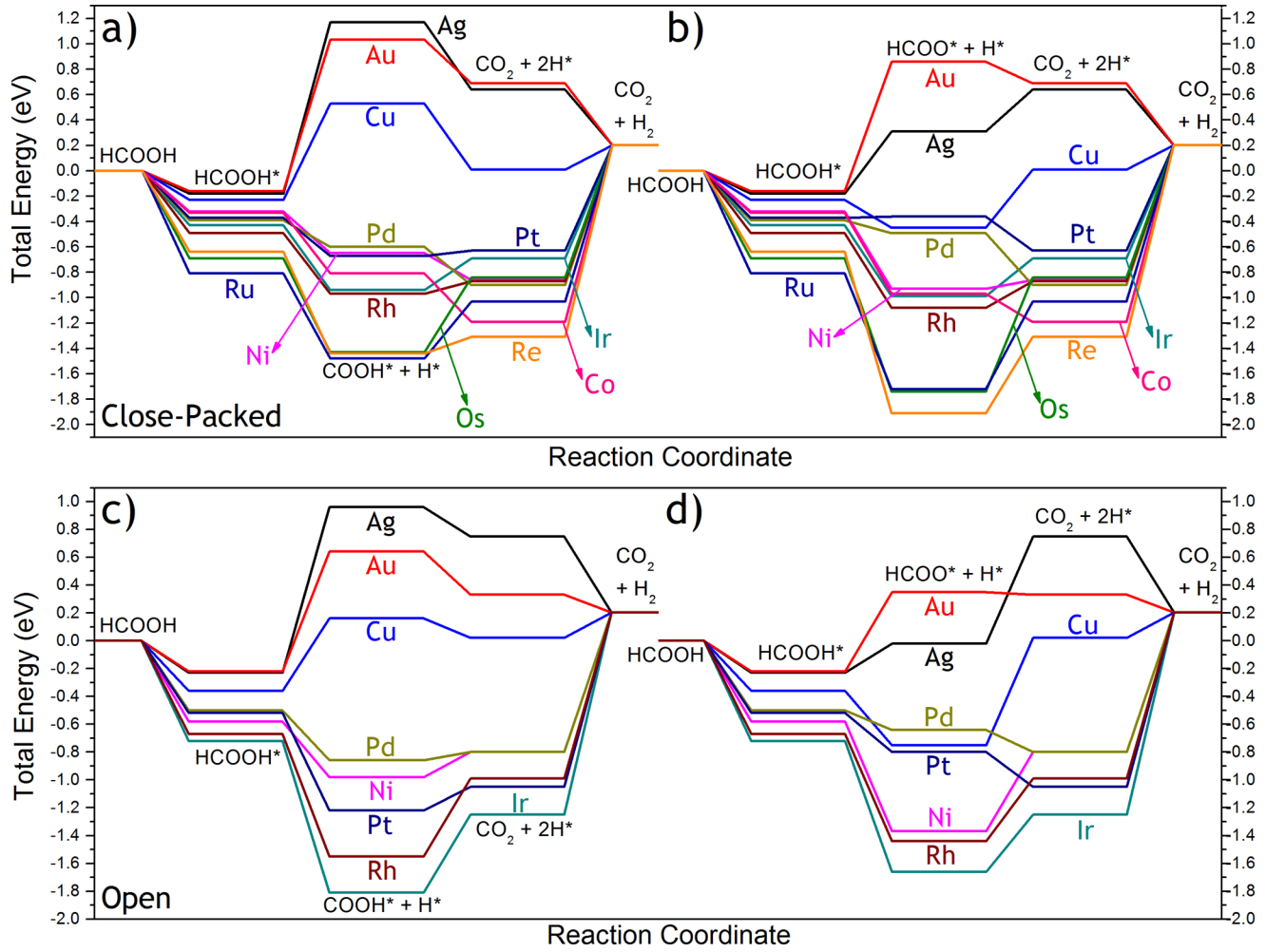

Figure 1. Thermochemical potential energy surfaces for formic acid dehydrogenation on close-packed fcc(111) and hcp(0001) facets and more open fcc(100) facets via carboxyl and formate intermediates. (a) carboxyl pathway on fcc(111) and hcp(0001) facets, (b) formate pathway on fcc(111) and hcp(0001) facets, (c) carboxyl pathway on fcc(100) facets, (d) formate pathway on fcc(100) facets. Energetics of surface reaction steps are calculated with all species at infinite separation from one another. Activation energy barriers are not included. Zero of the energy axis corresponds to HCOOH at infinite separation from the respective metal surface. Energies are not zero-point energy corrected.

derivatives of energy are calculated using a finite difference approximation.[51] A vibrational mode is considered dipole-active if a nonzero intensity is calculated from the gradient of the dipole moment (calculated using a finite difference approximation).[52] Binding energies calculated non self-consistently in RPBE[44] functional are provided in Table S2. Zero-point energy corrections for HCOOH(g), $CO_2(g)$, $H_2(g)$, HCOOH*, HCOO*, COOH*, H*, CO*, and OH* were calculated by assuming a quantum harmonic oscillator possessing the calculated vibrational frequencies. The zero-point energy correction was found to have minimal effect on the reaction energies of individual elementary steps. Therefore, they are presented in Table S3 for reference. The ZPE-corrected overall gas-phase reaction (HCOOH → CO_2 + H_2) energy is −0.06 eV, very close to the tabulated value of −0.15 eV.[53]

3. RESULTS AND DISCUSSION

The binding energies of HCOOH, HCOO, COOH, CO, OH, C, O, and H on the facets of the 12 metals studied are presented in Table 1. From the binding energies, we can draw some main conclusions about the structure sensitivity of adsorption on the metal surfaces studied. For HCOOH, HCOO, COOH, CO, OH, C, and O, the interaction with the (111) facet is weaker than with the (100) facet. In contrast, the difference in H binding on the two facets is within 0.1 eV for Ag, Pd, Cu, Ni, and Rh, whereas H binding is significantly stronger on the (100) facet of Pt and Ir. Furthermore, among the surfaces studied, we see that the binding of H does not vary as significantly as the other adsorbates, rather it falls into two major groups. On the coinage metals (Au, Ag, and Cu), the value is between −2.01 (Ag(100)) to −2.38 eV (Cu(111)), whereas it ranges between −2.70 (Pt(111)) and −3.04 eV (Re(0001)) for the rest of the metal surfaces studied.

In Scheme 1, we outline the steps for two pathways for formic acid dehydrogenation. Using the calculated binding energies of HCOOH, HCOO, COOH, and H on various metals and their facets, we develop potential energy surfaces for these two dehydrogenation pathways, as shown in Figure 1. Furthermore, in order to facilitate the discussion of the reactivity trends across the periodic table, we have illustrated the reaction energy ($\Delta E_{Reaction}$) of the dehydrogenation elementary steps in Figure 2. The results are also tabulated in the Supporting Information, Table S1.

3.1. Carboxyl Pathway. After adsorption of HCOOH, the first dehydrogenation reaction breaks either the C−H bond (forming COOH) or the O−H bond (forming HCOO). We

dx.doi.org/10.1021/cs500737p | ACS Catal. 2014, 4, 4434−4445

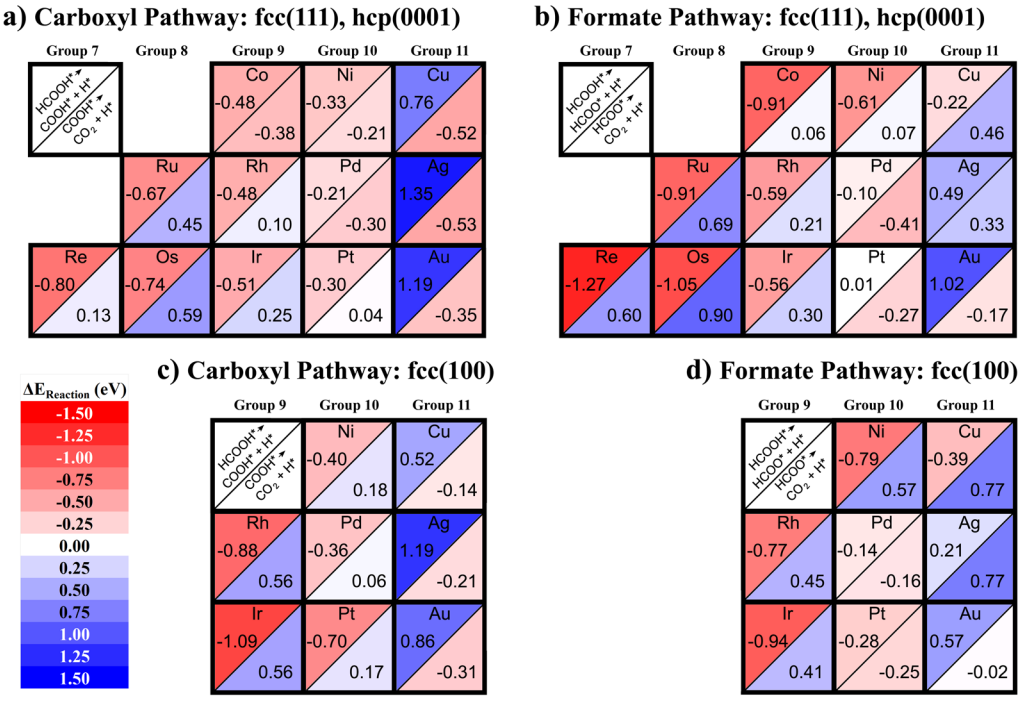

Figure 2. Reaction energies ($\Delta E_{Reaction}$) of HCOOH dehydrogenation elementary steps via formate-mediated and carboxyl-mediated pathways on close-packed and open facets, arranged according to placement on the periodic table. In (a) carboxyl pathway on fcc(111) and hcp(0001) facets, (b) formate pathway on fcc(111) and hcp(0001) facets, (c) carboxyl pathway on fcc(100) facets, and (d) formate pathway on fcc(100) facets. Each square corresponds to a metal facet and is subdivided into two halves. As indicated in the upper left box of each subfigure, the reaction energy for the first dehydrogenation step in a pathway is given in the upper left half, whereas the reaction energy for the second dehydrogenation step is given in the lower right half. The reaction energies are presented numerically (in eV) and by color-coding according to the legend. Energetics of reaction steps are calculated with all species adsorbed on the surface at infinite separation from one another.

will begin by discussing the reaction mechanism that starts with breaking the C−H bond, forming adsorbed carboxyl (COOH) and H on the surface.

3.1.1. HCOOH + * → COOH* + H**. On the close-packed facet, breaking the C−H bond in HCOOH is exothermic on Pt, Pd, Ni, Ir, Rh, Co, Ru, Re, and Os, while it is endothermic on Cu, Au, and Ag. If we consider how the reactivity varies across the periodic table (see Figure 2a), we see that breaking the C−H bond becomes more exothermic as we move from the right to the left within a period. On the other hand, we do not find any general trends when moving within each group of elements.

On the (100) facet (see Figure 2c), breaking the C−H bond in HCOOH is more exothermic on every metal studied, when compared with the close-packed facet of the same metal. Breaking that bond is exothermic on Ir(100), Rh(100), Ni(100), Pd(100), and Pt(100). As with the (111) facets, breaking the C−H bond in HCOOH is endothermic on Cu(100), Au(100), and Ag(100). For the open facet, we find trends which are similar to the close-packed facet: as we move from the right to the left within a period, the first dehydrogenation step becomes more exothermic.

The main conclusion from these trends is not so surprising. Following conventional wisdom, formic acid (a closed shell species) activation is easiest (i.e., most exothermic) on the open facets of reactive metals. Because formic acid is a closed-shell species, it is only weakly bound to metal surfaces, whereas the decomposition produces two strongly bound intermediates. Therefore, metals which are highly reactive will favor the decomposition reaction. On the periodic table, when moving within periods, the reactivity of the metals generally increases when moving to the left. Interestingly, we will show that a similar conclusion cannot be drawn for the second dehydrogenation reaction.

3.1.2. COOH → CO_2 + H**. Once the C−H bond in HCOOH is broken, the next step is to break the O−H bond in adsorbed COOH. First, considering the close-packed facets, we find that this step is endothermic (see Figure 2a) on Pt(111), Ir(111), Rh(111), Ru(0001), Re(0001), and Os(0001), while it is exothermic on Au(111), Ag(111), Cu(111), Pd(111), Ni(111), Co(0001). On (100) facets of the fcc metals studied (see Figure 2c), this elementary step is endothermic on Pd(100), Pt(100), Rh(100), Ir(100), and Ni(100), while it is exothermic on Cu(100), Ag(100), and Au(100). Overall, COOH dehydrogenation is more endothermic on the more open facet of every metal studied. This trend is the opposite of the first dehydrogenation step and is a result of how the surface structure affects the binding of different adsorbates nonuniformly. As explained earlier, COOH is stabilized on all metals on the (100) facet with respect to the (111) facet. On the other hand, the binding of H is not very structure sensitive, with the binding energy varying by ∼0.1 eV between the two facets. Therefore, because COOH* (the initial state of the elementary step) is stabilized on the more open facet while the product of the dehydrogenation step, H* (and CO_2, which is not adsorbed), is not significantly stabilized, the overall elementary step becomes more endothermic on the more open facet.

The trends with respect to the periodic table are notably different from the first dehydrogenation step. Here, we find that the reaction energy for COOH dehydrogenation becomes more endothermic on surfaces moving from the right to the left in a period, the opposite trend as before. The exceptions to these trends are for the Co(0001)/Ni(111) and Re(0001)/

dx.doi.org/10.1021/cs500737p | ACS Catal. 2014, 4, 4434−4445

Os(0001) pairs where the order is reversed. We do not find any discernible trends for the reactivity variation within groups in the periodic table.

The reason for this clear difference in trends is that in this elementary step, the reactant is a strongly bound species (COOH), while the product includes a gas-phase species (CO_2), which is not stabilized by the surface, and adsorbed H. Because there is a strongly adsorbed species in both the reactants and products, the behavior is governed by the trends in how these two intermediates are stabilized. We find that the binding energy of H varies from −2.01 (Ag(100)) eV to −3.04 eV (Re(0001)) over the metal surfaces studied. On the other hand, COOH binding varies from −1.19 eV (Ag(111)) to −3.22 eV (Ir(100)), a much larger range. As a result, as we move from the right to the left in the periodic table, COOH is stabilized to a greater degree than H, making the elementary step energetically more demanding.

3.2. Formate Pathway. An alternative to the carboxyl-mediated pathway is a formate-mediated pathway.

3.2.1. HCOOH + * → HCOO* + H**. In the formate pathway, the first dehydrogenation reaction breaks the O−H bond in HCOOH, thereby forming adsorbed HCOO. On the close-packed facet of the metals studied, this elementary step is exothermic on Cu, Pd, Ni, Ir, Rh, Co, Ru, Re, and Os, while it is endothermic on Pt, Au, and Ag. From Figure 2b, we see that the reaction energy becomes more exothermic on surfaces as we move from the right to the left within a period. In addition, we find that it becomes more exothermic as we move up within a group. This trend is most evident in groups 10 (Ni, Pd, and Pt) and 11 (Cu, Ag, and Au). However, there is an exception: Os(0001) and Ru(0001) display the opposite trend.

On the (100) facet, breaking the O−H bond is more exothermic than on the respective close-packed surface of every metal studied, as we also found for breaking the C−H bond in HCOOH; see section 3.1. O−H bond breaking is exothermic on Cu(100), Ir(100), Rh(100), Ni(100), Pt(100), and Pd(100). This step is endothermic on Au(100) and Ag(100), as it was for Au(111) and Ag(111). For the open facet, we find trends which are similar to the close-packed facet. That is, the elementary step becomes more exothermic when moving from the right to the left within a period. On the other hand, the trend within groups is less evident. Only group 11 follows the trend that the reaction becomes more exothermic moving up within the group.

The trends we find for this elementary step are similar to those for the first dehydrogenation step in the carboxyl pathway (HCOOH* → COOH* + H*). The main difference is that for this elementary step, we find trends within groups, which were not seen for carboxyl formation.

3.2.2. HCOO → CO_2 + H**. Once the O−H bond is broken, the next step is to break the remaining C−H bond in formate (HCOO*) to form CO_2 and H*. This step is endothermic on the close-packed facet of Ag, Cu, Ni, Rh, Ir, Co, Ru, Re, and Os, but exothermic on that of Au, Pt, and Pd. On the (100) facet of fcc metals, this step is endothermic on Ag, Cu, Ni, Rh, and Ir but is exothermic on Au, Pt, and Pd. In contrast to the O−H bond activation step, this elementary step is more endothermic on the more open facet than the close-packed facet of each metal. The reasoning is similar to that of the COOH decomposition step. Here, the open facet preferentially stabilizes HCOO*, while providing little stabilization for H*. The net result is that the initial state of the dehydrogenation (HCOO*) is stabilized relative to the final state (CO_2 + H*), leading to a more endothermic transformation on the open facet.

The trends across the periodic table for HCOO dehydrogenation are less well-defined than in the previous elementary steps. The trends found when moving within a period are not the same for all periods. In period 4 (Co, Ni, and Cu), HCOO* decomposition to CO_2 and H* becomes less endothermic when moving from the right (Cu) to the left (Co) on both facets. In period 5 (Ru, Rh, Pd, and Ag), the reaction is exothermic on Pd(111) and Pd(100), while it is endothermic on Ru(0001), Rh(111), Ag(111), Rh(100), and Ag(100). In period 6 (Re, Os, Ir, Pt, and Au), for close-packed facets, the reaction is exothermic on Au(111) and becomes more endothermic when moving to the left in the period (though it is more exothermic on Pt(111)). Also, the reaction is more endothermic on Os(0001) than Re(0001). For the (100) facets, the reaction energy is minimized (most exothermic) for Pt(100), is less exothermic on Au(100), and is endothermic on Ir(100).

Interestingly, the net result is that the surfaces which have the most exothermic reaction energy for HCOO dehydrogenation are in the middle of the periodic table, rather than to the left, as in the activation of formic acid, or to the right, as in the dehydrogenation of COOH. In particular, HCOO dehydrogenation is most exothermic on Pd(111) for the close-packed facets while it is most exothermic on Pt(100) for the open facets. Why is the behavior different from these other elementary steps? The behavior is similar to COOH decomposition in that the elementary step involves a strongly bound initial state (HCOO*) and a modestly bound final state (H*). The binding energy of HCOO varies across the periodic table from −1.78 eV (Au(111)) to −3.62 eV (Os(0001)), a more substantial range than H binding. As a result, the reaction energy (not its absolute value) *generally* increases to the left on the periodic table. However, there are significant deviations from this trend. The reason for these deviations is that, though the binding of HCOO varies in a similar magnitude as COOH over the surfaces studied, the rate of change across the table is not similar nor is it constant. In particular, Au(111) and Au(100) bind HCOO much weaker than any of the other surfaces studied. HCOO binding is relatively invariant for groups 9, 10, and 11 (except for Au), being ∼0.5 eV more stabilized relative to Au surfaces. In groups 8 and 7, the binding energy of HCOO strengthens again, by ∼0.5 and ∼1.0 eV, respectively. As a result, the reaction energy on Cu and Ag surfaces is more endothermic than on Ni and Pd, respectively, due to significantly weaker final state (H*) binding, rather than via stabilization of HCOO. In contrast, the reaction is only slightly more exothermic on Pt surfaces than Au surfaces because of the significant destabilization of HCOO on Au relative to Pt.

3.3. 2H* → H_2 + 2*. Finally, the last step in either pathway is H_2 recombinative desorption. As discussed earlier, the binding energy of H does not demonstrate substantial structure sensitivity for most of the metals studied (the difference in binding on the two facets is less than 0.1 eV). Notable exceptions are Pt and Ir, where the (100) facet binds H significantly stronger (by more than 0.2 eV) than the (111) facet. Additionally, we note that the binding energy is relatively invariant for the group 7, 8, 9, and 10 metals studied. Therefore, the reaction energy for H_2 recombinative desorption is similar on most of the metals studied (endothermic by ∼1.0 eV; see Figure 1), on either facet. In contrast to the behavior of these

dx.doi.org/10.1021/cs500737p | ACS Catal. 2014, 4, 4434−4445

metals, the binding energy of H is significantly weaker on the coinage metals. As a result, H_2 recombinative desorption is exothermic on Au and Ag surfaces, while being mildly endothermic on Cu surfaces; see Figure 1.

3.4. Catalytic Reactivity Trends. Can we draw any general conclusions from these analyses of individual elementary steps? The Sabatier principle states that the optimal catalyst for a reaction is one in which intermediates are bound with moderate strength. The optimal occurs with moderate binding strength due to the competing demands of the various elementary steps in a reaction mechanism. Therefore, in this section, we will demonstrate how balancing the trends in the energetics of individual elementary steps on metal surfaces, with respect to the surface structure and position of the metal in the periodic table, leads to optimal catalysts. First, in section 3.4.1, we consider the energetics of a subset of the reaction network, namely, the dehydrogenation steps. In section 3.4.2, we extend our analysis to include the entire potential energy surface to demonstrate how including additional elementary steps (i.e., HCOOH adsorption and hydrogen recombinative desorption) affects our initial conclusions. We note that recent work in the development of (universal) Brønsted−Evans−Polanyi relationships could be used with our thermochemical results to provide estimates for the kinetic barriers for these elementary steps.[54−56]

3.4.1. Dehydrogenation Energetics. In sections 3.1 and 3.2, we discussed how the reaction energy of the dehydrogenation elementary steps varies with respect to the position of the metal in the periodic table and the surface structure. Importantly, the first dehydrogenation step (producing HCOO or COOH from HCOOH, and thereby characterized by final-state-dominated energetics) becomes more exothermic (i.e., increasingly active) as the surface becomes more reactive and under-coordinated (we note that this trend would likely also hold for even more under-coordinated sites, including step edges), while the second dehydrogenation step, producing CO_2 + H, characterized by initial-state-dominated energetics, is more facile on active sites which are highly coordinated and relatively less reactive.

The consequences of these trends toward catalyst activity can be best understood in the context of Figure 2. When considering only the dehydrogenation elementary steps (i.e., Figure 2), materials which are very reactive (groups 7 and 8) or very inert (group 11) tend to have a highly exothermic step (seen with deep red in Figure 2), but consequently, they also have a subsequent highly endothermic step (seen with deep blue in Figure 2). Therefore, these materials will be limited by the activity of the endothermic step. Materials in the middle of the periodic table (groups 9 and 10) tend to have mildly endothermic or mildly exothermic steps, and their squares are colored close to white (though some actually have exothermic transition for both elementary steps). These are likely the most active catalysts, for the overall reaction, balancing the activity of sequential elementary steps.

By focusing on surfaces which have at most (an arbitrary) ΔE = 0.30 eV for both dehydrogenation steps in either the HCOO-mediated or COOH-mediated pathways, we find that the most promising surfaces are Rh(111), Ir(111), Co(0001), Ni(111), Pd(111), Pt(111), Ni(100), Pd(100), and Pt(100). In general, from this analysis, we find that a surface which shows favorable energetics for one of the pathways (HCOO- versus COOH-mediated) will also show favorable energetics on the other pathway. The main exception to this trend is Ni(100), which shows much more favorable energetics for the carboxyl pathway when compared with the formate pathway.

3.4.2. Overall Potential Energy Surfaces. In our initial analysis, we considered only the dehydrogenation steps, while the overall reaction coordinate also includes formic acid adsorption and hydrogen recombinative desorption. To evaluate how these additional steps affect the overall energetics on the surfaces studied, we consider the entire potential energy surface (see Figure 1). From the Sabatier principle, the optimal catalyst is the one whose potential energy surface deviates the least from a hypothetical straight line connecting the reactants' and products' potential energy levels. If the potential energy surface of a particular metal/facet deviates *below* this hypothetical line, this suggests that the particular metal/facet is too reactive. In this case, activating intramolecular bonds is relatively facile, while it is difficult to break surface−adsorbate bonds. This leads to a catalyst surface poisoned by the excessively strongly bound intermediates. On the other extreme, if the potential energy surface for a metal/facet deviates *above* this hypothetical line, then that metal/facet is too unreactive. In this case, poisoning by adsorbates/reaction intermediates is not the problem. Rather, it is difficult to activate stable molecules (or possibly a stable surface species). The optimal metal/facet should lie in between these two extreme cases.

On the basis of this principle, we qualitatively assess the surfaces studied using the potential energy surfaces shown in Figure 1. In general, we note that only Au(111), Au(100), Ag(111), and Ag(100) deviate above the hypothetical line connecting reactants to products. As such, we would expect activation of HCOOH to be difficult on these surfaces. Indeed, experimental studies have shown that Ag catalysts require preadsorbed oxygen to facilitate formic acid decomposition,[24] while rates on gold nanoparticles greater than ∼2 nm are low.[40,57] Cu, Pt, and Pd bind adsorbates modestly, and Pt and Pd have shown high dehydrogenation activity.[4,12,40] Rh, Ir, and Ni bind more strongly than Pt and Pd. Ir catalysts have shown high activity, while results on Rh have been mixed.[4,12] Co, Os, Ru, and Re bind adsorbates much more strongly than Pt and Pd. Therefore, we would expect them to be poisoned by various adsorbed species and/or possibly even be oxidized under realistic reaction conditions.

When we compare close-packed (111) to more open (100) facets of the fcc metals, we note that the potential energy surfaces are generally shifted downward. This is mainly a result of the stronger binding of HCOO and COOH to the more open facets. Notably, for Pt and Ir, hydrogen is significantly stabilized on their (100) facets with respect to their (111) facets, shifting their potential energy surface even further downward. Therefore, we would expect that the activity of more open facets for Au and Ag to be greater than the corresponding close-packed facets. The stronger binding on the more open facets makes the HCOOH activation steps more exothermic, and this should improve activity. The metals which already bind adsorbates strongly on the close-packed facet (i.e., Rh(111), Ir(111), and Ni(111)) will have this problem exacerbated on the more open facets, potentially leading to more severe poisoning by surface species.

The analysis of the entire thermochemical potential energy surfaces provides some different conclusions than the previous analysis that was based solely on the dehydrogenation elementary steps. In particular, Cu(111) and Cu(100) look more favorable, while Rh(111), Ir(111), Co(0001), Ni(100),

dx.doi.org/10.1021/cs500737p | ACS Catal. 2014, 4, 4434−4445

Table 2. Relative Stability of Isomeric Species: HCOO*, COOH*, CO_2(g) + H*, CO* + OH*, and CO* + O* + H* on All Surfaces Studied[a]

	relative energy (eV)									
	HCOO*		COOH*		CO_2 + H*		CO* + OH*		CO* + O* + H*	
Au(111)	0.00		0.17		−0.17	√	1.62		3.27	X
Ag(111)	0.00	√	0.86		0.32		1.57		3.23	X
Cu(111)	0.00	√	0.98		0.47		1.01		1.78	X
Pt(111)	0.00		−0.31	√	−0.27		0.15		0.44	X
Pd(111)	0.00		−0.11		−0.40	√	−0.18		0.08	X
Ni(111)	0.00		0.28	X	0.07		−0.43		−0.60	√
Ir(111)	0.00		0.05		0.30	X	0.17		−0.05	√
Rh(111)	0.00		0.10		0.21	X	−0.05		−0.28	√
Co(0001)	0.00		0.43	X	0.06		−0.36		−0.83	√
Os(0001)	0.00		0.31		0.90	X	0.12		−0.50	√
Ru(0001)	0.00		0.24		0.69	X	−0.04		−0.40	√
Re(0001)	0.00		0.46		0.60	X	−0.44		−1.84	√
Au(100)	0.00		0.30		−0.01	√	1.00		2.82	X
Ag(100)	0.00	√	0.98		0.77		1.29		2.87	X
Cu(100)	0.00	√	0.91		0.77		0.78		1.41	X
Pt(100)	0.00	X	−0.41		−0.24		−0.59	√	−0.07	
Pd(100)	0.00		−0.22		−0.16		−0.34	√	0.18	X
Ni(100)	0.00		0.39		0.57	X	−0.43		−0.67	√
Ir(100)	0.00		−0.15		0.41	X	−0.74		−0.88	√
Rh(100)	0.00		−0.11		0.44	X	−0.59		−0.68	√

[a]Values (in eV) are referenced relative to HCOO* (i.e., the relative stability of HCOO* is 0.00 eV), positive values are less stable than HCOO*, while negative values are more stable than HCOO*. The most stable isomer on each surface is indicated with a check mark, while the least stable isomer is indicated with an X mark. Metals are arranged according to periodic table group in descending order and, within each group, by decreasing atomic number.

and Pt(100) look less favorable than our initial analysis in section 3.4.1 suggested. This is due to the unfavorable energetics of H_2 recombinative desorption on all surfaces except Au(111), Au(100), Ag(111), and Ag(100). Though the binding energy of atomic H does not vary significantly over the group 7, 8, 9, and 10 surfaces studied, hydrogen recombinative desorption involves two H atoms, and therefore, the small differences in H binding become more significant when doubled. Considering both analyses, among the most promising monometallic surfaces would be Pt(111), Pd(111), Pd(100), Cu(111), and Cu(100).

Recently, Yoo and co-workers investigated formic acid decomposition on close-packed and stepped surfaces of monometallic catalysts through a combination of DFT calculations, scaling relations, and microkinetic modeling.[36] They predicted that the most active surfaces were Pt(111), Pd(111), Ir(111), Rh(111), and Ru(0001). These predictions are more in agreement with our earlier predictions (section 3.4.1), which were based solely on dehydrogenation thermochemistry, rather than our analysis involving the overall potential energy surfaces. That is, based on the entire potential energy surfaces, we predict Ir(111), Rh(111), and Ru(0001) to be less active than Pt(111) and Pd(111). They also predicted that the stepped (211) surfaces of Rh, Ir, and Ru would be orders of magnitude less active than the respective close-packed facets. We predict a similar trend for the (100) facets of Rh and Ir, which are more under-coordinated than their respective (111) facets.

There have been a number of experimental studies comparing the catalytic activity of monometallic catalysts. Sachtler and Fahrenfort developed a volcano curve between the temperature in which the activity reaches a fixed value versus heats of formation of bulk metal formates.[4] They ranked the catalysts from most to least active: Pt > Ir > Ru > Pd > Rh > Cu > Ni > Ag > Co > Au. One important caveat is that this ranking does not include a correction for the number of active sites (i.e., they did not calculate turnover rates). Solymosi et al. studied Pt group metals supported on Norit at 373 and 423 K, ranking the hydrogen turnover rates (values at 373 K given in parentheses) as Ir/Norit (0.096 s^{-1}) > Pt/Norit (0.064 s^{-1}) > Pd/Norit (0.044 s^{-1}) > Ru/Norit (0.013 s^{-1}) > Rh/Norit (0.009 s^{-1}).[12] Bulushev et al. studied Pd and Au supported catalysts and ranked the activity as Pd/C (0.071 s^{-1}) > Au/TiO_2 (0.016 s^{-1}) > Au/C (0.006 s^{-1}) at 373 K.[40] Ojeda and Iglesia suggested that well-dispersed Au clusters on Al_2O_3, which cannot be detected by TEM, can decompose HCOOH with higher metal-time yields than Pt.[37]

Due to the wide variety of experimental conditions and catalyst formulations (dispersion, support, etc.), it is difficult to make definitive conclusions on the basis of these results. However, we can draw some general conclusions from previously published work. Pt, Ir, and Pd have been shown to be active catalysts, while Au is generally inactive. The results on Pt, Pd, and Au agree with our assessment for these metals. That is, Pt (i.e., Pt(111)) and Pd (i.e., Pd(111) or Pd(100)) should be active, while Au (i.e., Au(111) or Au(100) should be inactive. In addition, the results from Ojeda and Iglesia are also consistent with the structure sensitivity that we found.[37] Our calculations predict that Au should be more active for formic acid decomposition on under-coordinated sites, which may include other under-coordinated sites that were not studied here, including steps and edges. Yet, we note that it is possible that even more under-coordinated sites of more reactive metals are too reactive and therefore poisoned by surface intermediates in the early stages of a reactor operation, thus contributing minimally to steady state reactivity of the catalyst.

dx.doi.org/10.1021/cs500737p | ACS Catal. 2014, 4, 4434−4445

Contrary to that, we cannot explain the relatively high experimental activity of Ir catalysts. Our results suggest that formic acid decomposition energetics on Ir(111) and Ir(100) are unfavorable. Furthermore, the energetics are very similar to that of Rh(111) and Rh(100), respectively. Yet, the experimental activity of Rh is reported as significantly lower than that of Ir. The answer to this puzzle may be found through a rigorous microkinetic analysis of a more comprehensive reaction network, including calculation of the activation energy barriers for the relevant elementary reaction steps and inclusion of reaction pathways leading to dehydration, in addition to dehydrogenation, which has been the focus of our analysis here. Further, systematic experimental studies allowing direct comparison of various catalysts as a function of active metal site alone, including particle size effects, are expected to offer valuable insights related to the structure sensitivity of HCOOH decomposition on iridium surfaces.

3.5. Carboxyl versus Formate Pathways. One important question that remains to be addressed is whether the formate-mediated or the carboxyl-mediated pathways are more active. To explore this question, first we examine the relative stability of HCOO and COOH on these surfaces. In Table 2 and Figure 3, we present the stability of isomeric species: HCOO*, COOH*, CO_2 + H*, CO* + OH*, and CO* + O* + H* on each of the surfaces studied. The results show that on the fcc(111) and hcp(0001) surfaces, HCOO is more stable than COOH on 10 of the 12 surfaces studied (every metal except Pt and Pd). On the fcc(100) surfaces, HCOO is more stable than COOH on 4 of the 8 surfaces studied (Ag, Au, Cu and Ni). These results may suggest that the HCOO-mediated pathway would be preferred on the close-packed facets of all metals except Pt and Pd and on the open facets of Ag, Au, Cu, and Ni. Alternatively, and depending of the experimental conditions, one might suggest that on the surfaces where HCOO is more stable than COOH, formate may be a most-abundant surface intermediate; however, it may not necessarily be the intermediate on the active pathway to dehydrogenation, but rather, it may play the role of a spectator species, occupying a significant fraction of the catalyst's surface.

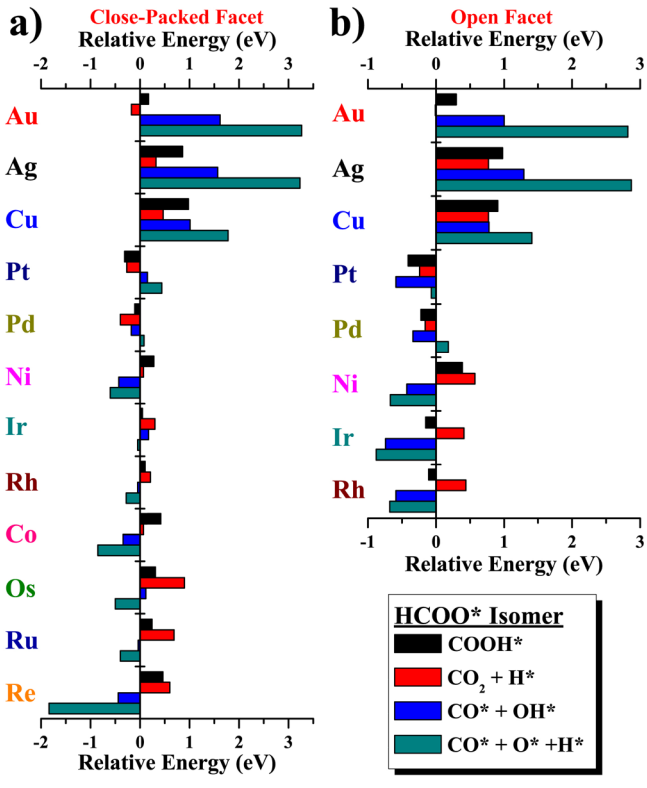

Figure 3. Stability of HCOO* isomers relative to HCOO*: COOH*, CO_2(g) + H*, CO* + OH*, and CO* + O* + H* on (a) close-packed facet of metals and (b) on (100) facets of elemental fcc metals. Values (in eV) are referenced relative to HCOO*, positive values are less stable than HCOO*; negative values are more stable than HCOO*. The relative stability of HCOO* is 0.00 eV for all cases. Metals are arranged according to periodic table group in descending order and, within each group, by decreasing atomic number.

As was discussed in detail earlier, the energetics of the first HCOOH dehydrogenation step and the second dehydrogenation step are balanced on surfaces with markedly different properties. If the first dehydrogenation step is facile on a surface, then the second dehydrogenation step is generally difficult. Conversely, if the first step is difficult on a surface, then the second step is often facile. The fundamental reason for this behavior is that in the first dehydrogenation step, an adsorbed intermediate (HCOO or COOH) is formed. If this intermediate is strongly bound, then the step is facile. In the second step, the intermediate must be removed, eliminating a closed-shell species (CO_2). If the intermediate was strongly bound, then consequently, this step would be difficult. As a result of this behavior, the stability of HCOO or COOH taken alone may be misleading indicators of the activity of a certain HCOOH dehydrogenation pathway. Therefore, we cannot definitively conclude which pathway may be more active on a particular surface without employing a full microkinetic model, taking into account reaction pressure, temperature, activation energy barriers, and entropic contributions.[58−60]

The analysis of the relative energetics of isomers can also provide some insights into the structure sensitivity of the reaction. For most of the metals studied, the most stable and the least stable isomers are the same on both (111) and (100) surfaces. Notable exceptions are Pt and Pd. On Pt(111), the most stable isomer is COOH*, and the least stable isomer is CO* + O* + H*. In contrast, the most stable isomer on Pt(100) is CO* + OH*, while the least stable isomer is HCOO*. On Pd(111), the most stable isomer is CO_2 + H*, while on Pd(100), the most stable isomer is CO* + OH*. When considering the other metals, though the most stable and least stable isomers do not change when comparing the two facets, on a particular metal, there are significant shifts in the relative stability of the adsorbates. In particular, highly decomposed isomers (i.e., CO* + OH*, CO* + O* + H*) are preferentially stabilized on the open facet of a metal, compared to what we find for the close-packed facet of the same metal.

3.6. Selectivity Between CO and CO_2 Production. Finally, we can also use the results presented in this isomer energetics analysis (Table 2 and Figure 3) to comment on the selectivity of HCOOH decomposition to CO_2 (dehydrogenation) versus CO (dehydration). If we consider a simple CO formation mechanism: HCOOH* → COOH* + H* → CO* + OH* + H*, then, the selectivity to CO is given by the selectivity of two key bifurcations in the overall decomposition mechanism. First, how selective is HCOOH decomposition to COOH (versus HCOO)? Second, if COOH were formed, how selective is the decomposition of COOH to CO + OH (versus dehydrogenation to CO_2 + H)? Based on these, we postulate that the criteria to form CO on a surface are (1) selectivity of

dx.doi.org/10.1021/cs500737p | ACS Catal. 2014, 4, 4434−4445

Table 3. Calculated and Experimental Dipole-Active Vibrational Frequency Modes of Adsorbed Formate (HCOO*) on Close-Packed Facets of Metals

	ν(C−H) (cm^{-1})	exptl (cm^{-1})	ν_s(OCO) (cm^{-1})	exptl (cm^{-1})	δ(OCO) (cm^{-1})	exptl (cm^{-1})	$\nu_\perp$ (cm^{-1})	exptl (cm^{-1})
Au(111)	2928	2896[a], 2824[a]	1304	1332[a]	731		243	
Ag(111)	2922	2936−2886[b]	1327	1260−1360[b]	730	752[b]	262	
Cu(111)	2975	2850−2864[c]	1328	1324−1326[c]	732		259	
Pt(111)	2990	2950[d]	1300	1340[d], 1315[e]	746	790[d]	294	
Pd(111)	2958	2904[f]	1314	1342[f], 1355[g]	734	792[f], 780[g]	293	340[g]
Ni(111)	3007	2915[h]	1328		747		294	
Ir(111)	3031	2847[i]	1315	1369[i]	747		322	
Rh(111)	3006	2910[j]	1318	1330[j]	735	790[j]	305	350[j]
Co(0001)	3020		1327		742		279	
Os(0001)	3036		1321		748		342	
Ru(0001)	3000	2910[k], 2939[m], 2933[n], 2917[o]	1323	1340[k], 1361[m], 1337[n], 1358[o]	733	810[k], 784[m], 807[o]	306	385[k], 382[o]
Re(0001)	3054		1320		727		339	

ν(C−H) is the C−H bond stretch, ν_s(OCO) is the symmetric C−O bond stretching, δ(OCO) is the symmetric deformation, and $\nu_\perp$ is a frustrated translation mode. [a]RAIRS[71] [b]RAIRS[77] [c]RAIRS[78] [d]HREELS[20] [e]RAIRS[79] [f]RAIRS[21] [g]HREELS[67] [h]SFG-spectroscopy[80] [i]FTIR, on Ir/SiO_2[12] [j]HREELS[17] [k]HREELS[81] [m]FTIR[82] [n]RAIRS[83] [o]EELS[16]

Table 4. Calculated and Experimental Dipole-Active Vibrational Frequency Modes of Adsorbed Formate (HCOO*) on fcc(100) Facets

	ν(C−H) (cm^{-1})	exptl (cm^{-1})	ν_s(OCO) (cm^{-1})	exptl (cm^{-1})	δ(OCO) (cm^{-1})	exptl (cm^{-1})	$\nu_\perp$ (cm^{-1})	exptl (cm^{-1})
Au(100)	2930		1317		728		240	
Ag(100)	2926		1334		724		241	
Cu(100)	2970	2840[a], 2910[a]	1339	1330[a]	738	760[a]	290	340[a]
Pt(100)	3004		1314		738		311	
Pd(100)	2975		1316	1340[b]	724	775[b]	276	270[b]
Ni(100)	3016	2948[c]	1273		713		216	
Ir(100)	3060		1318		736		345	
Rh(100)	3021		1322	1323[d]	725	758[d]	308	

ν(C−H) is the C−H bond stretch, ν_s(OCO) is the symmetric C−O bond stretching, δ(OCO) is the symmetric deformation, and $\nu_\perp$ is a frustrated translation mode. [a]EELS[26] [b]HREELS[64] [c]SFG-spectroscopy[84] [d]EELS[85]

HCOOH dehydrogenation to COOH and (2) selectivity of COOH decomposition to CO + OH.

To begin to answer this question, we look at the energetics of these competing elementary steps. For the first selectivity question (HCOOH → HCOO + H versus HCOOH → COOH + H), the difference in the thermochemistry of the competing steps is given by the relative stability of COOH* to HCOO*. COOH* is more stable than HCOO* on Pt(111), Pd(111), Pt(100), Pd(100), Rh(100), and Ir(100) and would make COOH formation preferred on these surfaces. For the second selectivity question, COOH* decomposition, we note that the initial states are again the same, and so we can compare the stability of the final states directly. The results show that CO_2 + H* is more stable on Au(111), Ag(111), Pd(111), Pt(111), Cu(111), Au(100), Ag(100), and Cu(100), while CO* + OH* is more stable on Co(0001), Ni(111), Rh(111), Ir(111), Ru(0001), Os(0001), Re(0001), Pd(100), Pt(100), Ni(100), Rh(100), and Ir(100). Therefore, if COOH were formed on these latter surfaces, we would predict significant HCOOH dehydration to CO. Interestingly, we find many more surfaces pass the second criteria for CO formation, rather than the first. As a consequence, even if a small fraction of the reaction flux proceeds through the carboxyl pathway, that flux will likely lead to dehydration products, and at least partial CO poisoning, depending on the reaction conditions.

The surfaces which pass both criteria are Pt(100), Pd(100), Rh(100), and Ir(100). As such, we would expect significant CO formation on these surfaces. Experiments have shown significant CO formation on Ru(0001),[61] Ni(100),[62] Ni(111),[63] Pd(100),[64−66] Pd(111),[67] Rh(111),[68] supported Re,[39] and supported Rh.[38,69] At 423 K, on Norit-supported metals, the selectivity to CO_2 decreased in the order Ir (99.0%) > Pt (98.0%) > Ru (97.3%) > Pd (95.1%) > Rh (91.8%).[12] Compared to these results, we see that our estimates based on this simple scheme are not perfect. We note that our estimates are only qualitative and that they treat selectivity as a binary function (either selective or unselective, while in reality the selectivity is a continuous function). As a result, for systems where the competing steps are very competitive (i.e., the isomers have similar stability), this analysis will be especially inaccurate. A comprehensive microkinetic model would be required to more rigorously answer the selectivity question, taking into account the reaction energetics, entropic contributions, as well as reaction conditions (pressure, temperature, and feed composition).

3.7. Where To Look for *COOH. Finally, we comment briefly on the search for the spectroscopically elusive *COOH intermediate, an intermediate that has been shown to play a key role in low temperature WGS reaction and the methanol synthesis reaction.[28,29,58,70−76] Based on the isomer energetics analysis, we see that *COOH is the most stable of all five isomers considered here only on Pt(111). Therefore, Pt(111) would be a good candidate surface to spectroscopically identify this species. Also, *COOH is more stable than HCOO* on Pd(111), Pd(100), Pt(100), Rh(100), and Ir(100). These may also be good candidate surfaces on which to find and identify

dx.doi.org/10.1021/cs500737p | ACS Catal. 2014, 4, 4434−4445

Table 5. Calculated Dipole-Active Vibrational Frequency Modes of Adsorbed Carboxyl (COOH*) on Close-Packed Facets of Metals

	ν(O−H) (cm^{-1})	ν(HOC-O) (cm^{-1})	δ(OH) (cm^{-1})	ν(HO−CO) (cm^{-1})	$\nu_\perp$ (cm^{-1})	$\nu_\perp$ (cm^{-1})
Au(111)	3464	1823	1199	1103	243	198
Ag(111)	3581	1770	1172	1051	177	150
Cu(111)	3741	1564	1204	1119	245	182
Pt(111)	3344	1748	1221	1124	283	256
Pd(111)	3312	1764	1200	1107	267	226
Ni(111)	3673	1516	1234	1125	309	225
Ir(111)	3696	1473	1259	1140	344	267
Rh(111)	3682	1497	1226	1127	330	249
Co(0001)	3687	1481	1214	1113	307	238
Os(0001)	3714	1429	1252	1129	356	276
Ru(0001)	3700	1488	1226	1129	361	245
Re(0001)	3694	1403	1237	1115	339	248

ν(O−H) is the O−H bond stretch, ν(HOC-O) is the HOC-O bond stretch, ν(HO−CO) is the HO−CO bond stretch δ(OH) is the in-plane O−H bond bend, and $\nu_\perp$ are frustrated translational modes.

Table 6. Calculated Dipole-Active Vibrational Frequency Modes of Adsorbed Carboxyl (COOH*) on fcc(100) Facets

	ν(O−H) (cm^{-1})	ν(HOC-O) (cm^{-1})	δ(OH) (cm^{-1})	ν(HO−CO) (cm^{-1})	$\nu_\perp$ (cm^{-1})	$\nu_\perp$ (cm^{-1})
Au(100)	3727	1721	1199	1112	226	237
Ag(100)	3799	1607	1180	1096	240	176
Cu(100)	3783	1545	1127	1211	282	209
Pt(100)	3720	1542	1144	1241	319	261
Pd(100)	3685	1387	1177	1063	253	221
Ni(100)	3717	1273	1017	1184	308	250
Ir(100)	3731	1457	1128	1254	389	277
Rh(100)	3695	1493	1124	1226	345	253

ν(O−H) is the O−H bond stretch, ν(HOC-O) is the HOC-O bond stretch, ν(HO−CO) is the HO−CO bond stretch δ(OH) is the in-plane O−H bond bend, and $\nu_\perp$ are frustrated translational modes.

COOH. In order to aid this experimental search, we present dipole-active vibrational frequencies for adsorbed HCOO (Table 3 and Table 4) and *COOH (Table 5 and Table 6) on all of the surfaces studied. The HCOO* results are compared with experimental results from the literature, when available. The techniques that have been used are (high-resolution) electron energy loss spectroscopy ((HR)EELS), reflection−absorption infrared spectroscopy (RAIRS), Fourier transform infrared spectroscopy (FTIR), and sum frequency generation spectroscopy (SFG). *COOH remains spectroscopically elusive, and therefore, we do not have any experimental comparisons to make.

4. CONCLUSIONS

We have presented a thermochemical analysis of formic acid decomposition on Au, Ag, Cu, Ni, Pd, Pt, Rh, and Ir fcc(111) and fcc(100), and Co, Ru, Os, and Re hcp(0001) single crystal surfaces, based on periodic, self-consistent DFT (GGA-PW91) calculations. More specifically, we presented calculated binding energies of important HCOOH decomposition intermediates including HCOO*, *COOH, *CO, *OH, *C, *O, and H* at their most stable adsorbed configurations. These binding energies are used to construct thermochemical potential energy surfaces for formic acid dehydrogenation via both the formate-mediated and the carboxyl-mediated pathways. We find that the first dehydrogenation step, producing COOH* or HCOO*, is most facile on under-coordinated sites of reactive metals (those on the left of the transition metals in the periodic table, e.g., Re, Ru, and Os). In contrast, the second dehydrogenation step, eliminating CO_2, is most driven on highly coordinated sites of relatively inert metals (those on the right of the transition metals in the periodic table, e.g. Cu, Ag, and Au). Based on this simple thermochemical analysis, and since the two dehydrogenation steps require markedly different catalyst properties, the optimal catalyst balances these requirements and lies therefore in the middle of the transition metals (e.g., Pt, Pd). Furthermore, we find that the structure of the surface affects the first and second dehydrogenation steps differently. The first dehydrogenation step is more exothermic, while the second dehydrogenation step is more endothermic when comparing the open facet with the close-packed facet of a particular metal. In contrast, recombinative desorption of H_2 has a similar reaction energy when comparing the two facets, except on Ir and Pt where it is more endothermic on the (100) facet. The relative stability of adsorbed COOH*, HCOO*, and other isomeric intermediates (i.e., CO* + OH*, CO_2 + H*, CO* + O* + H*) on these surfaces was calculated. These results provided insight into formic acid decomposition selectivity (dehydrogenation versus dehydration), and in conjunction with calculated vibrational frequency modes, these can guide the experimental community in designing experiments to successfully identify the elusive carboxyl (*COOH) intermediate with appropriate spectroscopic methods.

■ ASSOCIATED CONTENT

Supporting Information

The following file is available free of charge on the ACS Publications website at DOI: 10.1021/cs500737p.

Reaction energies and binding energies (PDF).

dx.doi.org/10.1021/cs500737p | ACS Catal. 2014, 4, 4434−4445

AUTHOR INFORMATION

Corresponding Author

*E-mail: manos@engr.wisc.edu.

Notes

The authors declare no competing financial interest.

ACKNOWLEDGMENTS

Research supported as part of the Institute for Atom-efficient Chemical Transformations (IACT), an Energy Frontier Research Center funded by the U.S. Department of Energy (DOE), Office of Science, Basic Energy Sciences (BES). We thank Prof. M. A. Barteau for inspiring discussions related to this project. The computational work was performed in part using supercomputing resources from the following institutions: EMSL, a National scientific user facility at Pacific Northwest National Laboratory (PNNL); the Center for Nanoscale Materials at Argonne National Laboratory (ANL); and the National Energy Research Scientific Computing Center (NERSC). EMSL is sponsored by the Department of Energy's Office of Biological and Environmental Research located at PNNL. CNM, and NERSC are supported by the U.S. Department of Energy, Office of Science, under contracts DE-AC02-06CH11357, and DE-AC02-05CH11231, respectively.

REFERENCES

(1) Bozell, J. J.; Petersen, G. R. *Green Chem.* **2010**, *12*, 539−554.
(2) Braden, D. J.; Henao, C. A.; Heltzel, J.; Maravelias, C. T.; Dumesic, J. A. *Green Chem.* **2011**, *13*, 1755−1765.
(3) Columbia, M. R.; Thiel, P. A. *J. Electroanal. Chem.* **1994**, *369*, 1−14.
(4) Sachtler, W. M. H.; Fahrenfort, J.. The Catalytic Decomposition of Formic Acid Vapour on Metals. Proceedings of the 2nd International Congress on Catalysis, Paris, France, 1960; p 831.
(5) Iglesia, E.; Boudart, M. *J. Catal.* **1983**, *81*, 224−238.
(6) Iglesia, E.; Boudart, M. *J. Catal.* **1983**, *81*, 204−213.
(7) Iglesia, E.; Boudart, M. *J. Catal.* **1983**, *81*, 214−223.
(8) Iglesia, E.; Boudart, M. *J. Catal.* **1984**, *88*, 325−332.
(9) Iglesia, E.; Boudart, M. *J. Phys. Chem.* **1986**, *90*, 5272−5274.
(10) Iglesia, E.; Boudart, M. *J. Phys. Chem.* **1991**, *95*, 7011−7016.
(11) Solymosi, F.; Zakar, T. S. *J. Mol. Catal. A-Chem.* **2005**, *235*, 260−266.
(12) Solymosi, F.; Koos, A.; Liliom, N.; Ugrai, I. *J. Catal.* **2011**, *279*, 213−219.
(13) Li, G. X.; Ridd, M. J.; Larkins, F. P. *Aust. J. Chem.* **1991**, *44*, 623−626.
(14) Gazsi, A.; Bansagi, T.; Solymosi, F. *J. Phys. Chem. C* **2011**, *115*, 15459−15466.
(15) Millar, G. J.; Rochester, C. H.; Waugh, K. C. *J. Chem. Soc. Farad. T.* **1991**, *87*, 1491−1496.
(16) Avery, N. R.; Toby, B. H.; Anton, A. B.; Weinberg, W. H. *Surf. Sci.* **1982**, *122*, L574−L578.
(17) Houtman, C.; Barteau, M. A. *Surf. Sci.* **1991**, *248*, 57−76.
(18) Toomes, R. L.; King, D. A. *Surf. Sci.* **1996**, *349*, 43−64.
(19) Jensen, M. B.; Myler, U.; Thiel, P. A. *Surf. Sci.* **1993**, *290*, L655−L661.
(20) Avery, N. R. *Appl. Surf. Sci.* **1982**, *11?2*, 774−783.
(21) Zheng, T.; Stacchiola, D.; Saldin, D. K.; James, J.; Sholl, D. S.; Tysoe, W. T. *Surf. Sci.* **2005**, *574*, 166−174.
(22) Madix, R. J.; Gland, J. L.; Mitchell, G. E.; Sexton, B. A. *Surf. Sci.* **1983**, *125*, 481−489.
(23) Haq, S.; Love, J. G.; Sanders, H. E.; King, D. A. *Surf. Sci.* **1995**, *325*, 230−242.
(24) Sexton, B. A.; Madix, R. J. *Surf. Sci.* **1981**, *105*, 177−195.
(25) Hayden, B. E.; Prince, K.; Woodruff, D. P.; Bradshaw, A. M. *Surf. Sci.* **1983**, *133*, 589−604.
(26) Sexton, B. A. *J. Vac. Sci. Technol.* **1980**, *17*, 141−142.
(27) Silbaugh, T. L.; Karp, E. M.; Campbell, C. T. *J. Am. Chem. Soc.* **2014**, *136*, 3964−3971.
(28) Gokhale, A. A.; Dumesic, J. A.; Mavrikakis, M. *J. Am. Chem. Soc.* **2008**, *130*, 1402−1414.
(29) Grabow, L. C.; Gokhale, A. A.; Evans, S. T.; Dumesic, J. A.; Mavrikakis, M. *J. Phys. Chem. C* **2008**, *112*, 4608−4617.
(30) Lin, C. H.; Chen, C. L.; Wang, J. H. *J. Phys. Chem. C* **2011**, *115*, 18582−18588.
(31) Gao, W.; Keith, J. A.; Anton, J.; Jacob, T. *Dalton T.* **2010**, *39*, 8450−8456.
(32) Yu, Y. L.; Wang, X.; Lim, K. H. *Catal. Lett.* **2011**, *141*, 1872−1882.
(33) Yue, C.; Lim, K. H. *Catal. Lett.* **2009**, *128*, 221−226.
(34) Gao, W.; Keith, J. A.; Anton, J.; Jacob, T. *J. Am. Chem. Soc.* **2010**, *132*, 18377−18385.
(35) Luo, Q. Q.; Feng, G.; Beller, M.; Jiao, H. J. *J. Phys. Chem. C* **2012**, *116*, 4149−4156.
(36) Yoo, J. S.; Abild-Pedersen, F.; Nørskov, J. K.; Studt, F. *ACS Catal.* **2014**, *4*, 1226−1233.
(37) Ojeda, M.; Iglesia, E. *Angew. Chem., Int. Ed.* **2009**, *48*, 4800−4803.
(38) Benitez, J. J.; Carrizosa, I.; Odriozola, J. A. *J. Chem. Soc. Farad. T.* **1993**, *89*, 3307−3312.
(39) Zheng, X.; Qian, Z. H.; Hattori, H. *B. Chem. Soc. Jpn.* **1991**, *64*, 3432−3437.
(40) Bulushev, D. A.; Beloshapkin, S.; Ross, J. R. H. *Catal. Today* **2010**, *154*, 7−12.
(41) Greeley, J.; Mavrikakis, M. *Nat. Mater.* **2004**, *3*, 810−815.
(42) Perdew, J. P.; Chevary, J. A.; Vosko, S. H.; Jackson, K. A.; Pederson, M. R.; Singh, D. J.; Fiolhais, C. *Phys. Rev. B* **1992**, *46*, 6671−6687.
(43) Greeley, J.; Nørskov, J. K.; Mavrikakis, M. *Annu. Rev. Phys. Chem.* **2002**, *53*, 319−348.
(44) Hammer, B.; Hansen, L. B.; Nørskov, J. K. *Phys. Rev. B* **1999**, *59*, 7413−7421.
(45) Properties of the Elements and Inorganic Compounds. In *CRC Handbook of Chemistry and Physics*, 95th ed.; Haynes, W. M., Bruno, T. J., Lide, D. R., Eds.; CRC Press: New York, 2015; pp 145−152.
(46) Chadi, D. J.; Cohen, M. L. *Phys. Rev. B* **1973**, *8*, 5747−5753.
(47) Monkhorst, H. J.; Pack, J. D. *Phys. Rev. B* **1976**, *13*, 5188−5192.
(48) Vanderbilt, D. *Phys. Rev. B* **1990**, *41*, 7892−7895.
(49) Bengtsson, L. *Phys. Rev. B* **1999**, *59*, 12301−12304.
(50) Neugebauer, J.; Scheffler, M. *Phys. Rev. B* **1992**, *46*, 16067−16080.
(51) Greeley, J.; Mavrikakis, M. *Surf. Sci.* **2003**, *540*, 215−229.
(52) Porezag, D.; Pederson, M. R. *Phys. Rev. B* **1996**, *54*, 7830−7836.
(53) Thermochemistry, Electrochemistry, and Solution Chemistry. In *CRC Handbook of Chemistry and Physics*, 95th ed.; Haynes, W. M., Bruno, T. J., Lide, D. R., Eds. CRC Press: New York, 2015; pp 19−20.
(54) Fajin, J. L. C.; Cordeiro, M. N. D. S.; Illas, F.; Gomes, J. R. B. *J. Catal.* **2014**, *313*, 24−33.
(55) Wang, S. G.; Temel, B.; Shen, J. A.; Jones, G.; Grabow, L. C.; Studt, F.; Bligaard, T.; Abild-Pedersen, F.; Christensen, C. H.; Nørskov, J. K. *Catal. Lett.* **2011**, *141*, 370−373.
(56) Bligaard, T.; Nørskov, J. K.; Dahl, S.; Matthiesen, J.; Christensen, C. H.; Sehested, J. *J. Catal.* **2004**, *224*, 206−217.
(57) Singh, S.; Li, S.; Carrasquillo-Flores, R.; Alba-Rubio, A. C.; Dumesic, J. A.; Mavrikakis, M. *AIChE J.* **2014**, *60*, 1303−1319.
(58) Grabow, L. C.; Mavrikakis, M. *ACS Catal.* **2011**, *1*, 365−384.
(59) Dumesic, J. A.; Rudd, D. F.; Aparicio, L. M.; Rekoske, J. E.; Trevino, A. A.*The Microkinetics of Heterogeneous Catalysis*; American Chemical Society: Washington, DC, 1993.
(60) Cortright, R. D.; Dumesic, J. A. *Adv. Catal.* **2002**, *46*, 161−264.
(61) Sun, Y. K.; Weinberg, W. H. *J. Chem. Phys.* **1991**, *94*, 4587−4599.
(62) Benziger, J. B.; Madix, R. J. *Surf. Sci.* **1979**, *79*, 394−412.
(63) Benziger, J. B.; Schoofs, G. R. *J. Phys. Chem.* **1984**, *88*, 4439−4444.

(64) Jorgensen, S. W.; Madix, R. J. *J. Am. Chem. Soc.* **1988**, *110*, 397−400.
(65) Sander, D.; Erley, W. *J. Vac. Sci. Technol. A* **1990**, *8*, 3357−3360.
(66) Solymosi, F.; Kovacs, I. *Surf. Sci.* **1991**, *259*, 95−108.
(67) Davis, J. L.; Barteau, M. A. *Surf. Sci.* **1991**, *256*, 50−66.
(68) Solymosi, F.; Kiss, J.; Kovacs, I. *J. Vac. Sci. Technol. A* **1987**, *5*, 1108−1109.
(69) Solymosi, F.; Erdohelyi, A. *J. Catal.* **1985**, *91*, 327−337.
(70) Liu, P.; Rodriguez, J. A. *J. Chem. Phys.* **2007**, *126*, 164705.
(71) Senanayake, S. D.; Stacchiola, D.; Liu, P.; Mullins, C. B.; Hrbek, J.; Rodriguez, J. A. *J. Phys. Chem. C* **2009**, *113*, 19536−19544.
(72) Rodriguez, J. A.; Evans, J.; Feria, L.; Vidal, A. B.; Liu, P.; Nakamura, K.; Illas, F. *J. Catal.* **2013**, *307*, 162−169.
(73) Vidal, A. B.; Feria, L.; Evans, J.; Takahashi, Y.; Liu, P.; Nakamura, K.; Illas, F.; Rodriguez, J. A. *J. Phys. Chem. Lett.* **2012**, *3*, 2275−2280.
(74) Lin, S.; Johnson, R. S.; Smith, G. K.; Xie, D. Q.; Guo, H. *Phys. Chem. Chem. Phys.* **2011**, *13*, 9622−9631.
(75) Yang, Y. X.; Evans, J.; Rodriguez, J. A.; White, M. G.; Liu, P. *Phys. Chem. Chem. Phys.* **2010**, *12*, 9909−9917.
(76) Gu, X. K.; Li, W. X. *J. Phys. Chem. C* **2010**, *114*, 21539−21547.
(77) Sim, W. S.; Gardner, P.; King, D. A. *J. Phys. Chem.* **1996**, *100*, 12509−12516.
(78) Nakamura, I.; Nakano, H.; Fujitani, T.; Uchijima, T.; Nakamura, J. *Surf. Sci.* **1998**, *402*, 92−95.
(79) Sawada, T.; Liu, Z. X.; Takagi, N.; Watanabe, K.; Matsumoto, Y. *Chem. Phys. Lett.* **2004**, *392*, 334−339.
(80) Kusafuka, K.; Noguchi, H.; Onda, K.; Kubota, J.; Domen, K.; Hirose, C.; Wada, A. *Surf. Sci.* **2002**, *502*, 313−318.
(81) Xie, J.; Mitchell, W. J.; Lyons, K. J.; Weinberg, W. H. *J. Chem. Phys.* **1994**, *101*, 9195−9197.
(82) Weisel, M. D.; Chen, J. G.; Hoffmann, F. M.; Sun, Y. K.; Weinberg, W. H. *J. Chem. Phys.* **1992**, *97*, 9396−9411.
(83) Barros, R. B.; Garcia, A. R.; Ilharco, L. M. *Surf. Sci.* **2005**, *591*, 142−152.
(84) Yuzawa, T.; Shioda, T.; Kubota, J.; Onda, K.; Wada, A.; Domen, K.; Hirose, C. *Surf. Sci.* **1998**, *416*, L1090−L1094.
(85) Gurney, B. A.; Ho, W. *J. Vac. Sci. Technol. A* **1987**, *5*, 632−634.